Supporting Information

Liang et al. 10.1073/pnas.1214900110

SI Text

SI Materials and Methods

Experiment Design. All participants first underwent a resting-state BOLD scan (8 min with 240 time points), and a resting-state ASL scan (7.5 min with 50 pairs of control and label images), which were randomized across the group. During the resting-state runs, participants were instructed to remain as still as possible with their eyes closed. In addition, 39 of the participants also underwent a BOLD scan and an ASL scan while performing an *N*-back working-memory (WM) task. The orders for BOLD and ASL scans were randomized across the subjects. Previously, the data were used to study regional brain activity during resting and task states (1). The task was presented as a block paradigm with four conditions: three active WM tasks (1-back, 2-back, and 3-back) and a low-level vigilance task (0-back). In the vigilance task, following the instruction "press for D," participants pressed one button each time the letter D (or d) appeared on the screen. In the three active WM task conditions, following the instruction "N back" (where $n = 2$), participants pressed a button when the current letter shown on the screen matched the one presented "N" items back. The task included six runs, with one 0-back, 1-back, 2-back, and 3-back block in each run and took a total of about 27 min. Each block lasted 62 s and contained a 2-s instruction indicating task difficulty level followed by 30 consecutive trials of single letter stimuli (500-ms duration; 1,500-ms interstimulus interval). Each run therefore lasted 4 min and 24 seconds beginning with an 8-s fixation followed by the 0-back block and then the randomized 1-, 2-, and 3-back blocks. Additional 8-s fixation occurred at the end of each run. Visual stimuli were presented and responses were collected using E-Prime (Psychology Software Tools, Inc.). The stimuli were back-projected on a screen inside the scanner using an LCD projector. The reason we adopted separate scans for ASL and BOLD is to get higher SNR and larger spatial coverage for ASL scans, which was facilitated by the pseudo-continuous arterial spin labeling (pCASL) sequence.

Data Acquisition. Scanning was performed on a 3 Tesla Siemens Allegra MR Scanner (Siemens) equipped with a quadrature volume head coil. High-resolution anatomical images were acquired using a 3-D MPRAGE T1-weighted sequence with 160 slices, 1.0-mm isotropic voxels, repetition time (TR) = 2,500 ms, echo time (TE) = 4.38 ms, flip angle (FA) = 8°. Functional BOLD images were acquired using a gradient-echo EPI sequence with TR = 2000 ms, TE = 27 ms, FA = 77°, thirty-nine 4-mm slices without interslice gap, field of view (FOV) = 220 × 220 mm^2, and an in-plane resolution of 3.44 × 3.44 mm^2. Functional ASL data were acquired using a pseudocontinuous arterial-spin–labeling (pCASL) technique. Interleaved control and label images were acquired using a gradient echo EPI sequence with TR = 4,500 ms, TE = 21 ms, FA = 90°, twenty 5-mm slices with 20% gap, FOV = 220 × 220 mm^2, and an in-plane resolution of 3.44 × 3.44 mm^2, labeling duration = 1.6 s, label offset = 80 mm, postlabeling delay = 1.2 s, and bipolar gradients = 9 s/mm^2. During the WM task, TR of pCASL sequence was adjusted to 4 s to better fit the duration of task blocks and bipolar gradient was reduced to 2 s/mm^2 with minimum TE as 13 ms. Other parameters were the same as those of the resting-state scan. Head movement was minimized using individually custom-made foam padding, and earplugs were used to attenuate scanner noise.

Image Preprocessing. Both BOLD and ASL images were preprocessed using the AFNI software package (3), which are briefly outlined as follows.

BOLD imaging. Data preprocessing of both resting state and task state included slice-timing correction, head-motion correction, linear trend removal, temporal band-pass filtering (0.01–0.1 Hz), and spatially smoothing (FWHM = 6 mm). Before the preprocessing we removed the first four volumes of resting-state data to allow for signal to reach a steady state. Task-state BOLD series of each run was divided into separate conditions (0-back, 1-back, 2-back, and 3-back) as follows: for each 60 s block in each run, the first four volumes (8 s) were discarded and two volumes (4 s) of the next block were included to minimize the effects of hemodynamic delay from previous conditions (4). Then, all BOLD data were aligned to their corresponding T1-weighted images, and normalized BOLD images were created by applying the transformation of T1-weigthed images to the ICBM452 template. Finally, several nuisance variables, including six head-motion parameters, the global brain signal, the averaged signal from white matter and ventricles, were removed by multiple linear regression analysis.

ASL imaging. For resting-state and task-state ASL data preprocessing, a control/label image with the fewest outliers was chosen from the entire resting-state or task-state scan session as a reference for motion correction, and were linearly registered to each other. Then control and label images in resting state and in each run of task state were separately realigned to their reference images. Following spatial smoothing (FWHM = 6 mm), CBF-weighted time series were created by pairwise subtraction of the label and control images. After these, for each run in task-state, images in each condition (0-back, 1-back, 2-back, and 3-back) were extracted from their corresponding blocks. Then, absolute rCBF time series were approximated using a one-compartment model (5), and averaged together to get individual-level absolute rCBF maps. Finally, rCBF maps were aligned to their corresponding T1-weighted images and then normalized into the standard Talairach space by applying the abovementioned transformation of T1-weigthed images to ICBM452 template.

Network Analysis. ***Functional hubs.*** Hubs were mapped by computing FCS. For resting-state data, the BOLD time course of each voxel within the predefined GM mask was first extracted and a correlation matrix is calculated. Because the removal of global signal mathematically induces negative correlations and remains controversial (6, 7), we restricted our analysis to positive correlations unless otherwise stated. For each subject, the resulted correlation matrix with negative correlations set to zero was directly applied as a weighted network G with N nodes. FCS at a given voxel x_0 was computed as the average of functional connectivity between x_0 and all other voxels in the brain. Voxels with high FCS (>mean) were identified as functional hubs, representing that they were of high connectivity to the rest of the brain. Two other nodal centrality measures, efficiency and betweenness, were also computed to identify functional hubs. For a given node i, the efficiency is computed as $E_i = \frac{1}{N-1} \sum_{j \neq i \in G} \frac{1}{l_{i,j}}$, where $l_{i,j}$ is the shortest path length between node i and j. Nodal efficiency measures the ability of a node to propagate information with the other nodes in a network. The betweenness for a given node i is calculated as $B_i = \sum_{m \neq i \neq n \in G} \frac{\sigma_{mn}(i)}{\sigma_{mn}}$, where σ_{mn} is the total number of shortest paths from node m to node n and $\sigma_{mn}(i)$ is the number of

shortest paths from node m to node n that pass through node i. Betweenness captures the influence that a node has over the flow of information between all other nodes in a network. To further explore the influence of physical distance on FCS–rCBF relationship, at a given voxel x_0, we also computed short-range and long-range FCS. The former was computed as the average correlation between x_0 and a set of voxels, to which the Euclidean distance (approximately physical distance) were less than 75 mm from voxel x_0. The latter was computed as the average correlation between x_0 and another set of voxels that were more than 75 mm from x_0. For task data, at each condition, voxelwise correlations of BOLD time courses were computed within each block and then averaged across the six runs in the same condition. FCS was then examined using the same strategy as for the resting-state data. For computational efficiency, we down-sampled the data to 4-mm isotropic voxels (a total of 16,589 voxels in GM).

Modular analysis. Modules refer to a set of nodes that are highly interconnected but less connected with the rest of the network (8). Detection of modular structure in the brain system can help identify groups of brain regions that are associated with specific functions. A group-weighted brain network was obtained by averaging graphs across all subjects, and subjected to modular analysis. We use the Louvain algorithm, which is a fast and accurate community detection algorithm for large networks (9).

After module detection, we determined the within-module FCS in each identified module as the average functional connectivity between a given voxel and all other voxels within its own module. The resulted within-module FCS in each module was then normalized as follows:

$$Z_{FCS}(i) = \frac{FCS(i) - \overline{FCS}}{\sigma(FCS)},$$

where $FCS(i)$ is the within-module FCS of a node i in module s. $\overline{FCS}$is the average within-module FCS of all nodes in module s. $\sigma(FCS)$ is the SD of within-module FCS of all nodes in module s.

rCBF/FCS ratio analysis. To evaluate the metabolic consumption per unit connectivity strength, we computed the ratio of rCBF to FCS. Regions with higher rCBF/FCS ratio tend to have higher metabolic demands to connect them to the rest of the brain. For interindividual comparison purpose, the rCBF/FCS ratio maps for each subject were standardized to z scores using the following formula:

$$Z_{rCBF/FCS}(i) = \frac{rCBF/FCS(i) - \overline{rCBF/FCS}}{\sigma(rCBF/FCS)},$$

where $\overline{rCBF/FCS}$ is the mean rCBF/FCS across all of the voxels within the GM mask, and $\sigma(rCBF/FCS)$is the SD within the GM mask.

Relationship Between Functional Network Connectivity and rCBF. For each participant, both FCS and rCBF values were standardized to z scores so that they could be averaged and compared across subjects (10). To quantitatively evaluate the relationship between FCS and rCBF, we performed correlation analyses across voxels and across participants (11, 12) for both resting and task data. To further identify the contributions of physical distance to the FCS–rCBF relationship in resting brains, for each participant, we separately computed the across-voxel correlation between rCBF and short- and long-range FCS. After Fisher's transforming the two sets of correlation coefficients to z scores, a paired t test was performed to evaluate in which distance range the FCS would be more correlated with rCBF. Across-subject correlation analysis was performed at each voxel within the GM mask to investigate the relationship between rCBF and short- and long-range FCS at rest, respectively. The threshold for across-subject correlation maps was set to a corrected $P < 0.05$ (which corresponded to an uncorrected single voxel significance level of $P < 0.05$ and a minimum cluster size of 3,840 mm^3).

It has been demonstrated that regional rCBF is related to both GM volume (13) and structural network connectivity (14), thus the relationship between functional network connectivity and rCBF could result from a common underlying morphological basis. To exclude the potential role of anatomical structures in explaining the FCS–CBF relationship at rest, gray matter volume (GMV) and structural connectivity strength (SCS) were computed from T1-weighted images. In brief, segmentation was performed using unified segmentation model developed in SPM8 (15). The rigidly aligned gray matter and white matter images were further aligned using a nonlinear registration algorithm (DARTEL) (15). A custom template was created based on the registration results and each individual's GM images were transformed to the DARTEL template space, modulated by the determinant of the Jacobian of the transformation. Finally, modulated GM images were transformed to Talairach space using AFNI and spatial smoothed with Gaussian kernel of 6 mm. For each voxel, SCS was computed as the average of correlations of GM volume between that particular voxel and the rest voxels in the GM mask across subjects (16). Across-voxel correlation analyses were separately performed between rCBF and GM volume or SCS. Furthermore, we also calculated a partial correlation between rCBF and FCS across voxels, controlling for the effects of GM volume or SCS.

To evaluate the task effects of increasing working-memory load on the relationship between FCS and rCBF, the across-voxel correlations were converted to z scores using Fisher's transformation to allow for paired t tests between every two pairs of the four task states. Using Bonferroni correction for multiple testing, the significance threshold was set at $0.05/6 = 0.0083$. To further estimate the task effect on rCBF/FCS ratio, the normalized rCBF/FCS maps for each task state were included in a voxel-by-voxel repeated-measures ANOVA model, with task load as a within-subject fixed effect, to identify significantly modulated brain regions during WM tasks. The threshold was set to a corrected $P < 0.05$ (which corresponded to an uncorrected single voxel significance level of $P < 0.05$ and a minimum cluster size of 3,840 mm^3). Subsequently, paired t tests were performed on the average rCBF/FCS values of the significantly modulated brain regions during WM tasks between different task loads. Bonferroni-corrected significance threshold was set at $0.05/6 = 0.0083$.

Brain–Behavior Relationship at Working-Memory Task States. To test whether WM task-related changes in FCS and rCBF might correlate with behavioral performance, we conducted voxelwise correlation analyses between changes in FCS and rCBF and behavior performance, dprime, which is a measurement of hit rate that penalizes for the false alarm rate (17). Task-related changes in rCBF or FCS was calculated as rCBF or FCS under each level of WM conditions divided by rCBF or FCS under baseline (0-back); behavioral performance was accordingly calculated as the ratio of dprime under each task load to that under 0-back. The analyses were performed for the 2-back and 3-back conditions only, as performance in the 1-back condition was at ceiling. Brain–behavior correlation analyses at each load condition were conducted within masked regions that showed significant task activation or deactivation in FCS ($P_{corrected} < 0.05$) or rCBF ($P_{corrected} < 0.001$). The rationale of using a task activation/deactivation mask was to ensure that regions showing the brain–behavior relationship colocalized within significant task regions. The threshold was set to $P < 0.05$ (uncorrected single voxel significance level of $P < 0.05$ and a minimum cluster size based on the size of the activation/deactivation mask of each load).

Validation Analysis. To evaluate the reliability of our results, we examined the influences of different preprocessing and analysis strategies. First, we explored the possible effects of global signal removing, given that the removal of global signal is associated with the emergence of negative correlations, which are still difficult to interpret (6, 18, 19). Second, several studies have shown that network parameters could vary considerably across different spatial scale of node parcellation (20–22), we thus evaluated the spatial resolution effects on connectivity strength by down-sampling the resting-state data to 8-, 12-, and 16-mm isotropic voxels. Third, we examined the influence of different connection inclusion criteria on the resulting FCS. Given the disagreements in treating negative correlations in R-fMRI network studies (6, 7, 23), we recomputed FCS based on the whole correlation matrices consisting of both positive connections and negative connections (absolute values). Given that the weak correlations among voxels could be attributing to signal noise, we also recomputed FCS on the correlation matrices including only the strong connections ($r > 0.25$) and repeated all of the analyses.

Head-Motion Analysis. To moderate the effects of head motion on estimates of functional connectivity, we censored volumes within each subject's fMRI time series that were associated with sudden head motion (24). For each subject, fMRI volume was censored if its derivative values have a Euclidean norm above 0.35. Eleven out of 48 subjects had motion censoring according to the above criteria and all of them had more than 125 frames (~5 min) of data remaining after motion censoring. We recalculated FCS and short-/long-range FCS using censored time courses, and all our previous observations remain hold: (*i*) FCS and rCBF highly correlated ($r = 0.45$, $P < 0.0001$); (*ii*) both short-range ($r = 0.29$, $P < 0.001$) and long-range ($r = 0.57$, $P < 0.0001$) FCS were significantly correlated with rCBF, with the long-range FCS–rCBF correlation higher than the short-range FCS–rCBF correlation ($P = 0.008$).

1. Zou Q, et al. (2012) Intrinsic resting-state activity predicts working memory brain activation and behavioral performance. *Hum Brain Mapp*, 10.1002/hbm.22136.
2. Kahnt T, Chang LJ, Park SQ, Heinzle J, Haynes J-D (2012) Connectivity-based parcellation of the human orbitofrontal cortex. *J Neurosci* 32(18):6240–6250.
3. Cox RW (1996) AFNI: Software for analysis and visualization of functional magnetic resonance neuroimages. *Comput Biomed Res* 29(3):162–173.
4. Mostofsky SH, et al. (2009) Decreased connectivity and cerebellar activity in autism during motor task performance. *Brain* 132(Pt 9):2413–2425.
5. Wang J, et al. (2005) Amplitude-modulated continuous arterial spin-labeling 3.0-T perfusion MR imaging with a single coil: Feasibility study. *Radiology* 235(1):218–228.
6. Murphy K, Birn RM, Handwerker DA, Jones TB, Bandettini PA (2009) The impact of global signal regression on resting state correlations: Are anti-correlated networks introduced? *Neuroimage* 44(3):893–905.
7. Fox MD, Zhang D, Snyder AZ, Raichle ME (2009) The global signal and observed anticorrelated resting state brain networks. *J Neurophysiol* 101(6):3270–3283.
8. Newman ME (2006) Modularity and community structure in networks. *Proc Natl Acad Sci USA* 103(23):8577–8582.
9. Blondel V, Guillaume J, Lambiotte R, Lefebvre E (2008) Fast unfolding of communities in large networks. *J Stat Mech* 10:10008.
10. Buckner RL, et al. (2009) Cortical hubs revealed by intrinsic functional connectivity: Mapping, assessment of stability, and relation to Alzheimer's disease. *J Neurosci* 29(6):1860–1873.
11. Mennes M, et al. (2010) Inter-individual differences in resting-state functional connectivity predict task-induced BOLD activity. *Neuroimage* 50(4):1690–1701.
12. Mennes M, et al. (2011) Linking inter-individual differences in neural activation and behavior to intrinsic brain dynamics. *Neuroimage* 54(4):2950–2959.
13. Várkuti B, et al. (2011) Quantifying the link between anatomical connectivity, gray matter volume and regional cerebral blood flow: An integrative MRI study. *PLoS ONE* 6(4):e14801.
14. Hagmann PC, et al. (2008) Mapping the structural core of human cerebral cortex. *PLoS Biol* 6(7):e159.
15. Ashburner J (2007) A fast diffeomorphic image registration algorithm. *Neuroimage* 38(1):95–113.
16. He Y, Chen ZJ, Evans AC (2007) Small-world anatomical networks in the human brain revealed by cortical thickness from MRI. *Cereb Cortex* 17(10):2407–2419.
17. Haatveit BC, et al. (2010) The validity of d prime as a working memory index: Results from the "Bergen n-back task" *J Clin Exp Neuropsychol* 32(8):871–880.
18. Weissenbacher A, et al. (2009) Correlations and anticorrelations in resting-state functional connectivity MRI: A quantitative comparison of preprocessing strategies. *Neuroimage* 47(4):1408–1416.
19. Liang X, et al. (2012) Effects of different correlation metrics and preprocessing factors on small-world brain functional networks: A resting-state functional MRI study. *PLoS ONE* 7(3):e32766.
20. Fornito A, Zalesky A, Bullmore ET (2010) Network scaling effects in graph analytic studies of human resting-state FMRI data. *Front Syst Neurosci* 4:22.
21. Zalesky A, et al. (2010) Whole-brain anatomical networks: Does the choice of nodes matter? *Neuroimage* 50(3):970–983.
22. Wang J, et al. (2009) Parcellation-dependent small-world brain functional networks: A resting-state fMRI study. *Hum Brain Mapp* 30(5):1511–1523.
23. Wang JH, et al. (2011) Graph theoretical analysis of functional brain networks: Test-retest evaluation on short- and long-term resting-state functional MRI data. *PLoS ONE* 6(7):e21976.
24. Power JD, Barnes KA, Snyder AZ, Schlaggar BL, Petersen SE (2012) Spurious but systematic correlations in functional connectivity MRI networks arise from subject motion. *Neuroimage* 59(3):2142–2154.

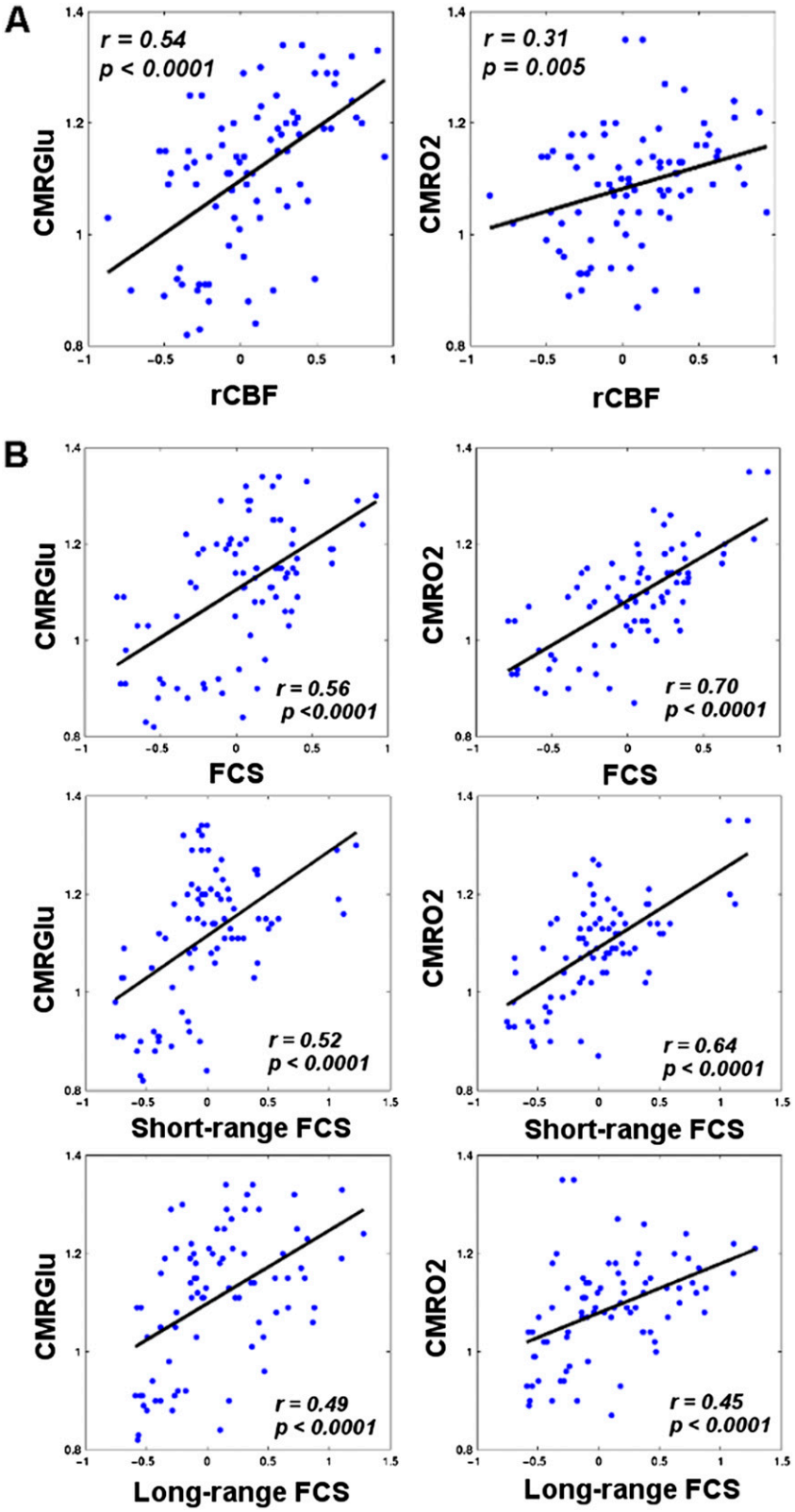

Fig. S1. Scatterplot of the spatial correlations across Brodmann areas between PET-derived metabolism measures and (*A*) rCBF and (*B*) FCS, short-range and long-range FCS at resting state.

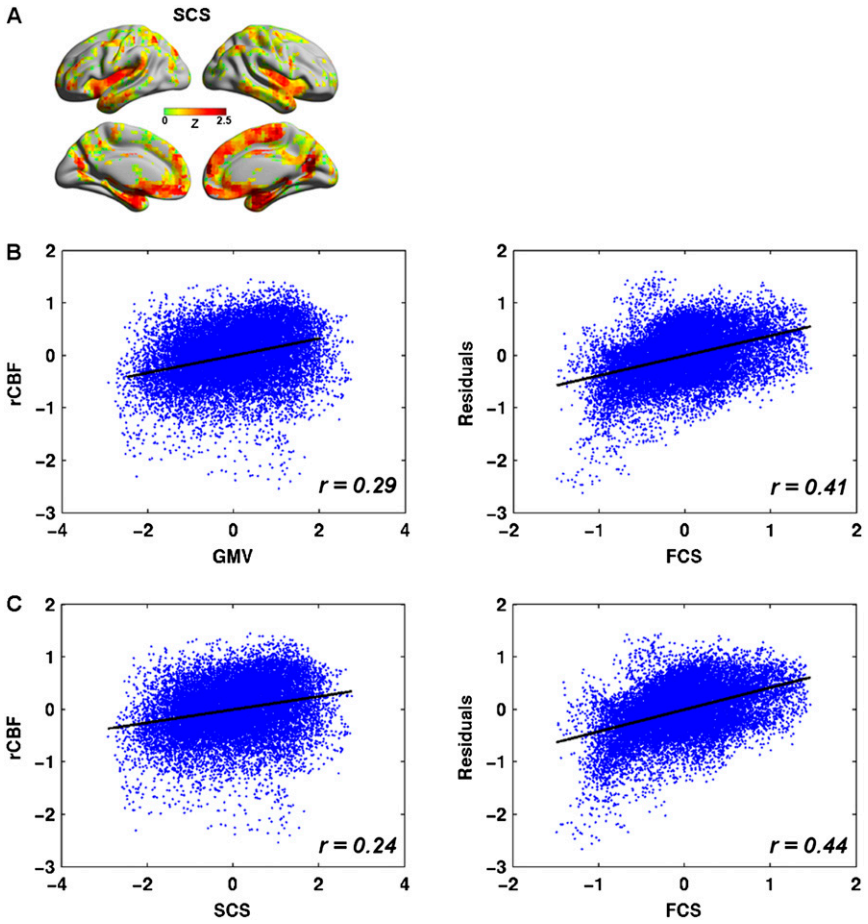

Fig. S2. Role of structural variables. (*A*) Map of SCS. (*B*) Scatterplot of GMV and rCBF (*Left*) and its residuals plotted against FCS (*Right*). (*C*) Scatterplot of SCS against rCBF (*Left*) and its residuals plotted against FCS (*Right*).

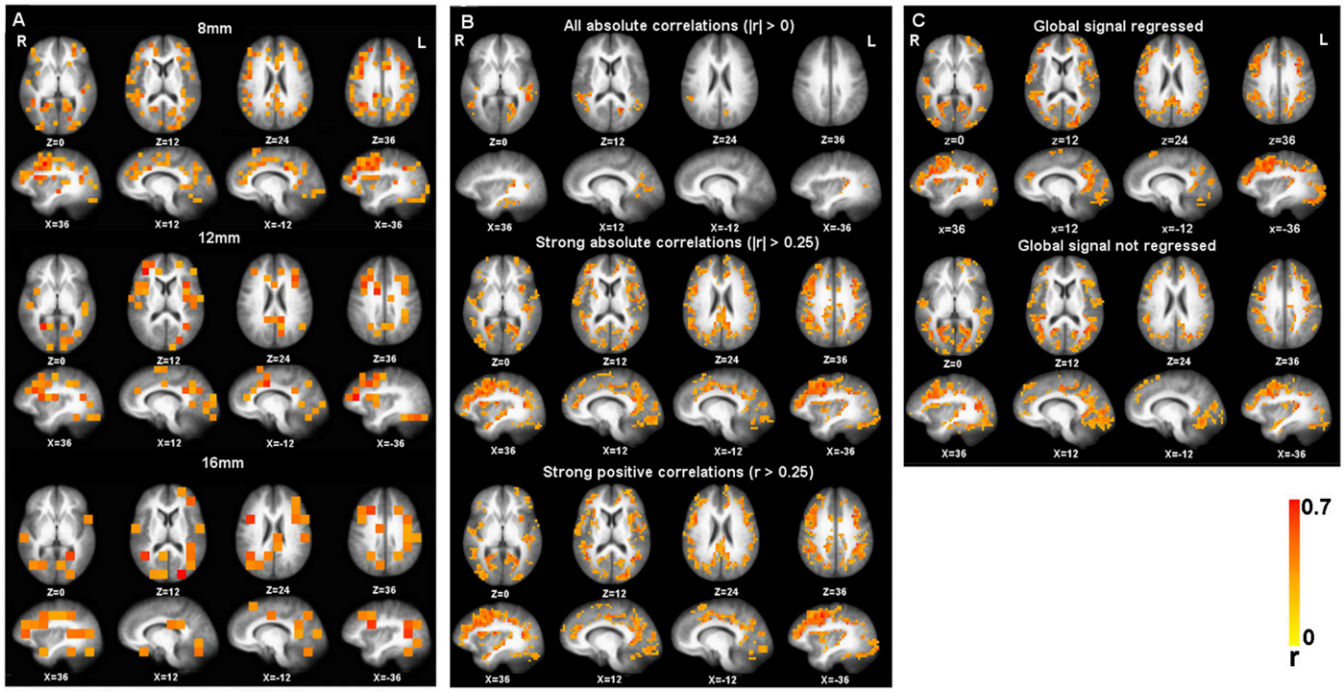

Fig. S3. Across-subject correlations between rCBF and FCS in validation analyses. (*A*) Effects of different spatial resolutions. (*B*) Effects of different connection criteria while controlling negative and weak ($r < 0.25$) functional correlations. (*C*) Effects of global brain signal.

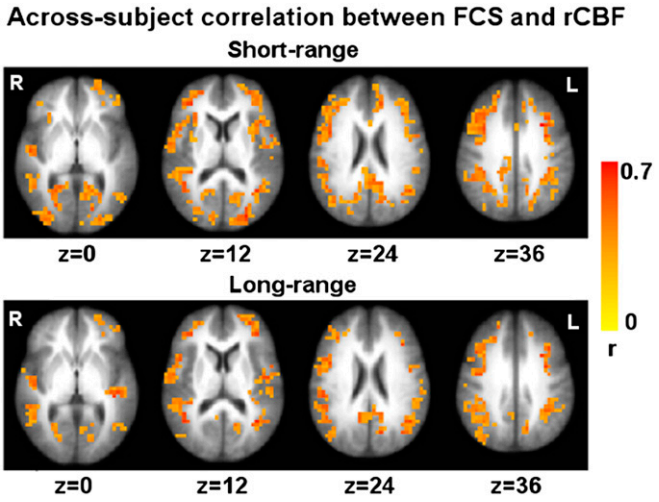

Fig. S4. Across-subject correlation between rCBF and short-range and long-range FCS.

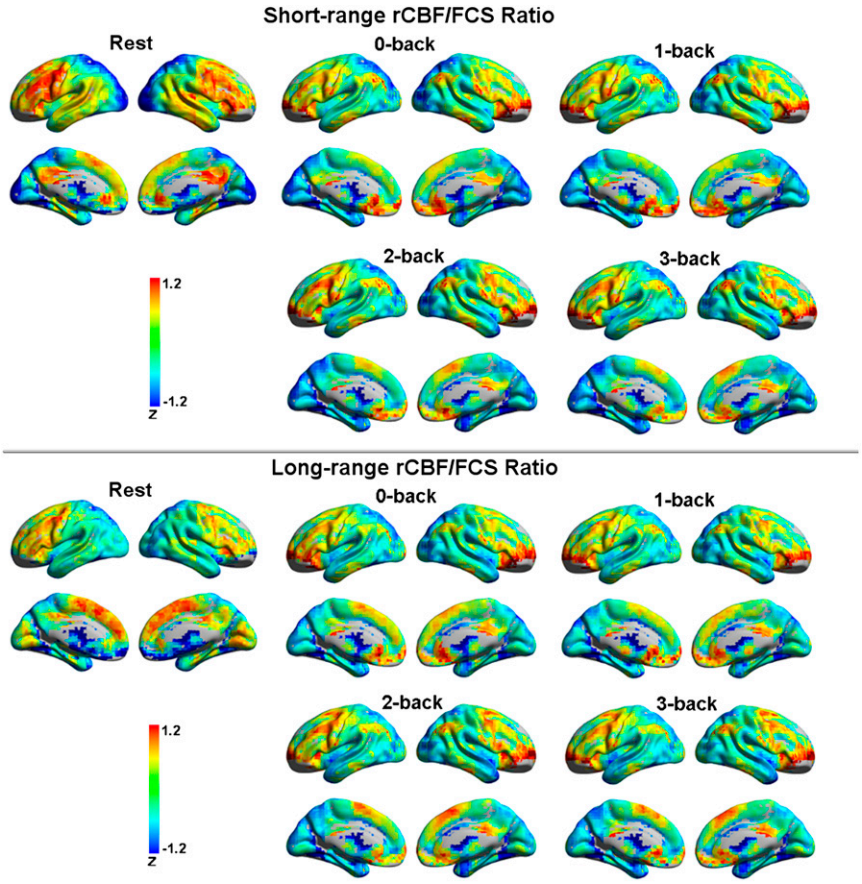

Fig. S5. Distance-dependent rCBF/FCS ratio map at resting and working-memory task states.

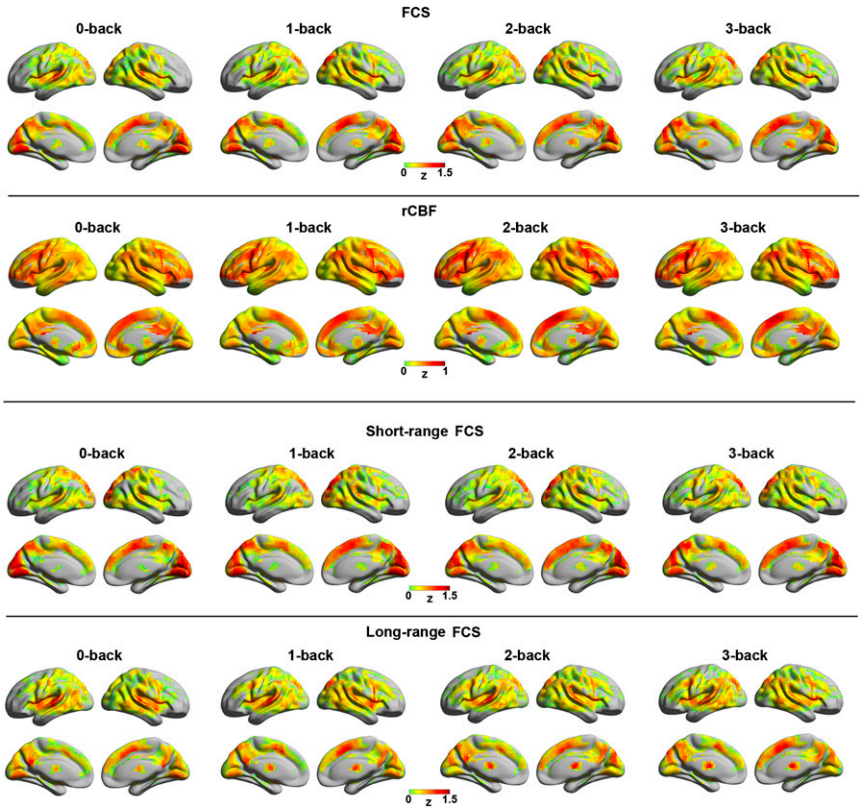

Fig. S6. Maps of (*A*) functional hubs, (*B*) rCBF, and (*C*) short-range and (*D*) long-range hubs at working-memory task states.

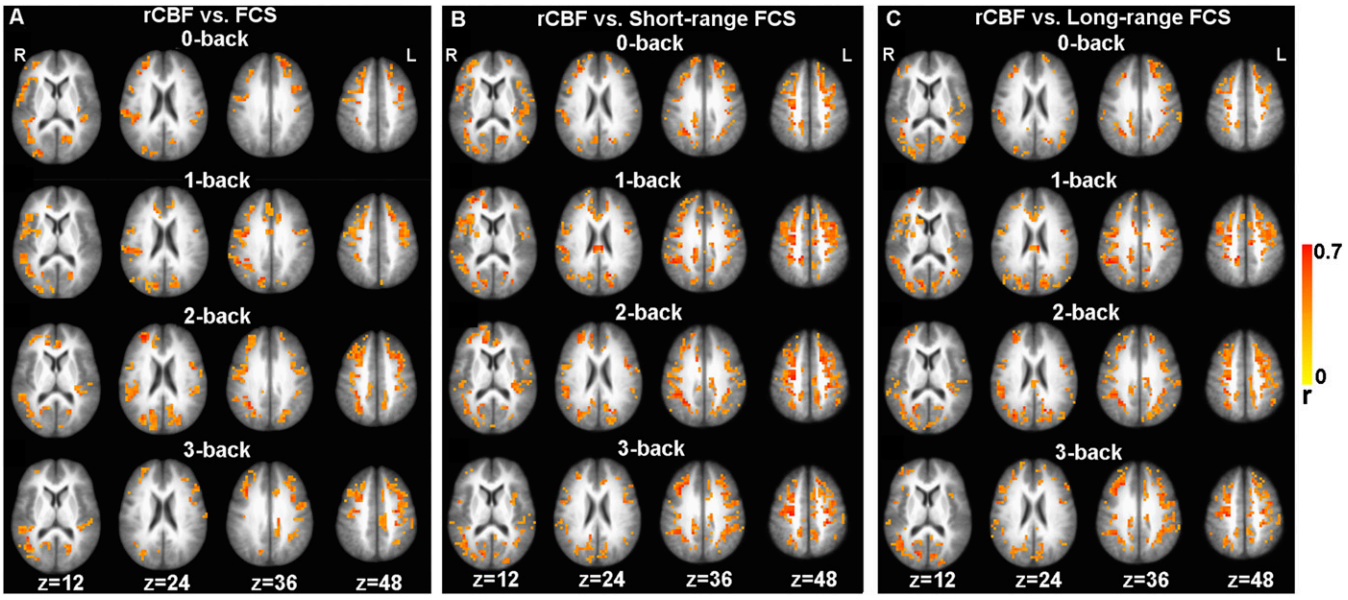

Fig. S7. Across-subject FCS–rCBF correlations at working-memory task states. (*A*) rCBF vs. FCS. (*B*) rCBF vs. short-range FCS. (*C*) rCBF vs. long-range FCS.

Table S1. Across-voxel correlations between FCS and rCBF without global signal regression

	Without global signal regression	
Brain metrics	*r*	*P*
FCS vs. rCBF	0.41	<0.0001
SCS vs. rCBF	0.25	<0.0001
FCS vs. rCBF (control for SCS)	0.39	<0.0001
GMV cs. rCBF	0.29	<0.0001
FCS vs. rCBF (control for GMV)	0.35	<0.0001

Table S2. Across-voxel correlations between FCS and rCBF under different spatial resolutions

	8		12		16	
Brain metrics	*r*	*P*	*r*	*P*	*r*	*P*
FCS vs. rCBF	0.46	<0.0001	0.43	<0.0001	0.50	<0.0001
SCS vs. rCBF	0.19	<0.0001	0.18	<0.0001	0.20	<0.0001
FCS vs. rCBF (control for SCS)	0.44	<0.0001	0.42	<0.0001	0.50	<0.0001
GMV cs. rCBF	0.28	<0.0001	0.24	<0.0001	0.24	<0.0001
FCS vs. rCBF (control for GMV)	0.41	<0.0001	0.40	<0.0001	0.48	<0.0001

Table S3. Across-voxel correlations between FCS and rCBF under different connection inclusion criteria

	All absolute correlations		Strong absolute correlations		Strong positive correlations	
Brain metrics	*r*	*P*	*r*	*P*	*r*	*P*
FCS vs. rCBF	0.30	<0.0001	0.35	<0.0001	0.31	<0.0001
SCS vs. rCBF	0.26	<0.0001	0.16	<0.0001	0.10	<0.0001
FCS vs. rCBF (control for SCS)	0.25	<0.0001	0.35	<0.0001	0.31	<0.0001
GMV cs. rCBF	0.29	<0.0001	0.29	<0.0001	0.29	<0.0001
FCS vs. rCBF (control for GMV)	0.28	<0.0001	0.31	<0.0001	0.27	<0.0001